Electronic Supplementary Information

for

**Self-assembling diacetylene molecules on atomically flat insulators**

*Elisseos Verveniotis[1], Yuji Okawa[1], Marina V. Makarova[1,2], Yasuo Koide[3], Jiangwei Liu[3], Břetislav Šmíd[3,4], Kenji Watanabe[3], Takashi Taniguchi[3], Katsuyoshi Komatsu[1], Takeo Minari[1], Xuying Liu[1], Christian Joachim[1,5], Masakazu Aono[1]*

[1]International Center for Materials Nanoarchitectonics (WPI-MANA), National Institute for Materials Science (NIMS), 1-1 Namiki, Tsukuba, Ibaraki 305-0044, Japan
[2]Institute of Physics, Czech Academy of Sciences, Na Slovance, 2, Prague 8, 18221, Czech Republic
[3]National Institute for Materials Science (NIMS), 1-1 Namiki, Tsukuba, Ibaraki 305-0044, Japan
[4]International Institute for Carbon-Neutral Energy Research (WPI-I$^2$CNER), Kyushu University, Nishi-ku, Fukuoka 819-0395, Japan
[5]Centre d'Elaboration de Matériaux et d'Études Structurales (CEMES), Centre National de la Recherche Scientifique (CNRS), 29 rue J. Marvig, 31055 Toulouse Cedex, France

## Experimental Details

### X-Ray photoelectron Spectroscopy

X-ray photoelectron spectroscopy (XPS) was performed in an ultrahigh vacuum (UHV) experimental chamber equipped with a Theta Probe by Thermo Electron Co. with two-dimensional multichannel spectroscopic detector and monochrome X-ray source (Al Kα, 1486.6 eV). All binding energies were referenced to the energy of the C $1s$ peak at 285.0 eV. Atomic composition of each sample calculated based on atomic sensitivity factors are displayed in respective survey spectra[1]. Peak separation was performed by KolXPD software[2]. Unless mentioned otherwise, all spectra were fitted with a combination of Gaussian and Lorentzian profile after subtraction of a Shirley type background[3].
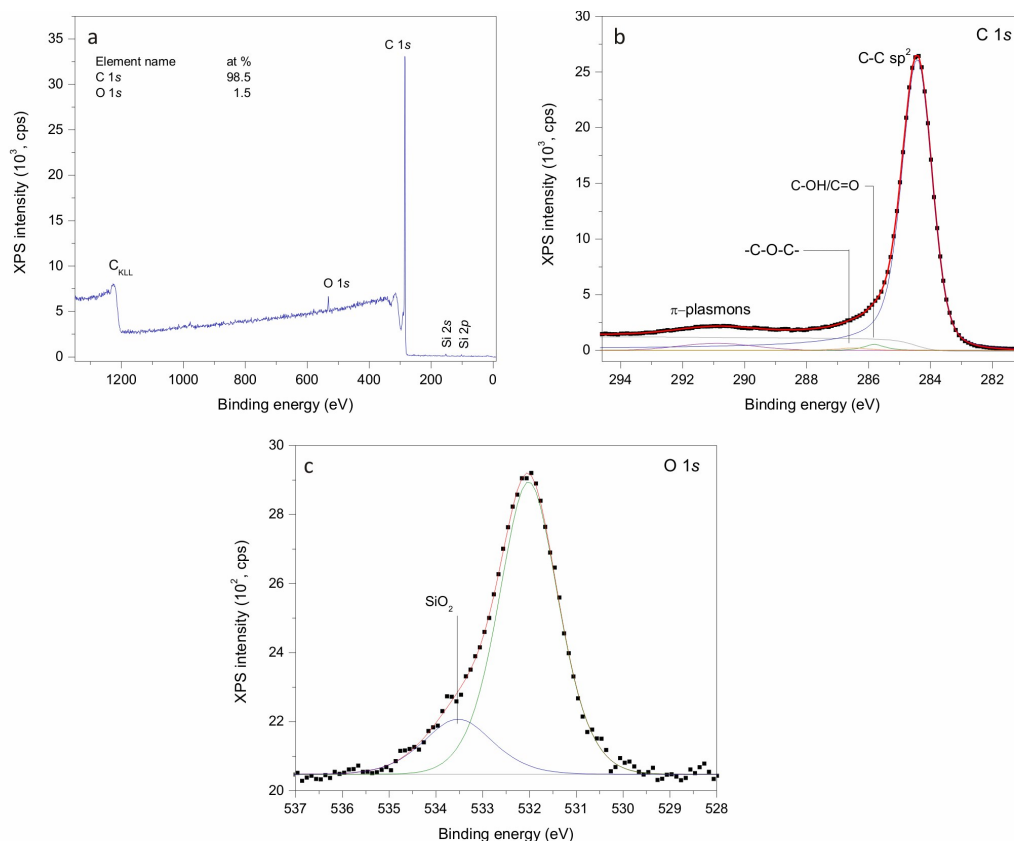
## Results

### XPS

*Sample 1 – HOPG*

The survey spectrum and core level spectra of C $1s$ and O $1s$ are displayed in Figures S1a, b and c, respectively. For the main component of C $1s$ peak we used Doniach-Sunjic function in convolution with Gaussian peak. The asymmetric parameter a in our case equals to 0.052, which is in agreement with previous studies[4,5].

The corresponding spectrum shown in Figure S1c reveals a main peak in the O $1s$ region at 531.9 eV that can be assigned to carbonyl functional group on the graphite surface[6]. The minor peak at binding energy of 533.5 could be assigned to ether type groups –C–O–C– on the HOPG surface. A small contribution can be found in C $1s$ peak as well. On the survey scan in Figure S1a we can also see evidence for small (negligible) traces of Si.

**Figure S1** XPS data collected on the surface of HOPG: (a) survey spectrum, (b) C 1*s* and (c) O 1*s* deconvoluted core level spectra.


*Sample 2 – MoS$_2$*

The survey spectrum measured on the MoS$_2$ surface is displayed in Figure S2a. According to the XPS results in Figures S2b and c, Mo 3$d_{3/2}$, Mo 3$d_{5/2}$, S 2$s$, S 2$p_{1/2}$ and S 2$p_{3/2}$ peaks were observed at 232.5, 229.3, 226.5, 163.4, and 162.2 eV, respectively. Deconvolution of the Mo 3$d$ region by peak fitting revealed a Mo 3$d$ doublet at a position indicative of Mo in a 4+ oxidation state[7]. We examined the S 2$p$ region, which was fitted with one distinct doublet. This shows the hexagonal semiconducting phase in MoS$_2$[8]. Carbon and oxygen are presented on the surface as a natural contamination – see Figures S2d and e. In the case of C 1$s$ and O 1$s$ peaks the linear background subtraction was necessary to use prior fitting the peaks.

2
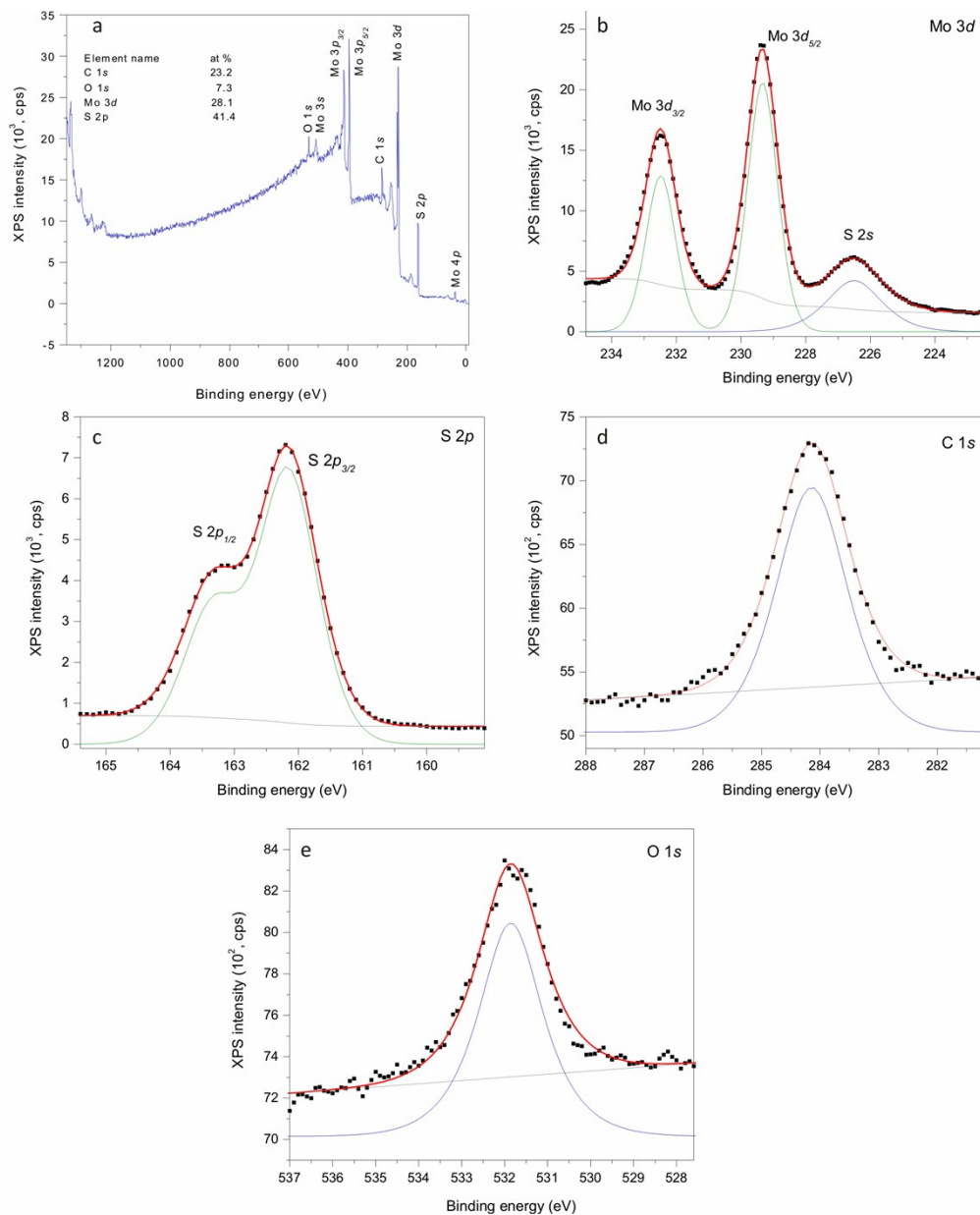
**Figure S2** XPS (a) survey spectrum, (b) Mo 3$d$, (c) S 2$p$, (d) C 1$s$ and (e) O 1$s$ data measured on surface of $MoS_2$ sample.

*Sample 3 – Sapphire*

Data measured on the $Al_2O_3$ sample can be seen in Figure S3. Survey spectrum is displayed in Figure 3a. Two peaks were fitted to Al 2$p$ spectra (Figure S3b). The peak on binding energy at 74.2 eV was assigned to $Al_2O_3$[9]. Corresponding O 1$s$ peak is detected as main peak at the binding energy of 531.3 eV as shown in Figure 3c.

The peak on binding energy at 72.3 eV was assigned to zeolite salt $Na_2Al*Si_2O_6*H_2O$. It also corresponds to the Na 1$s$ binding energy at 1072.8 eV displayed in Figure 3d.

Small amount of $NaC_2O_4$ is suspected to exist due to the binding energy of Na 1$s$ at 1070.8 eV and C 1$s$ at 289 eV. Another C 1$s$ peak shown in Figure 3e at binding energy of 287.2 eV is a

contribution from C=O bond. Trace amount of Si is detected but not further analyzed by XPS. Suspected SiC (or any other carbide) may exist due to the C 1*s* peak at 283 eV binding energy.
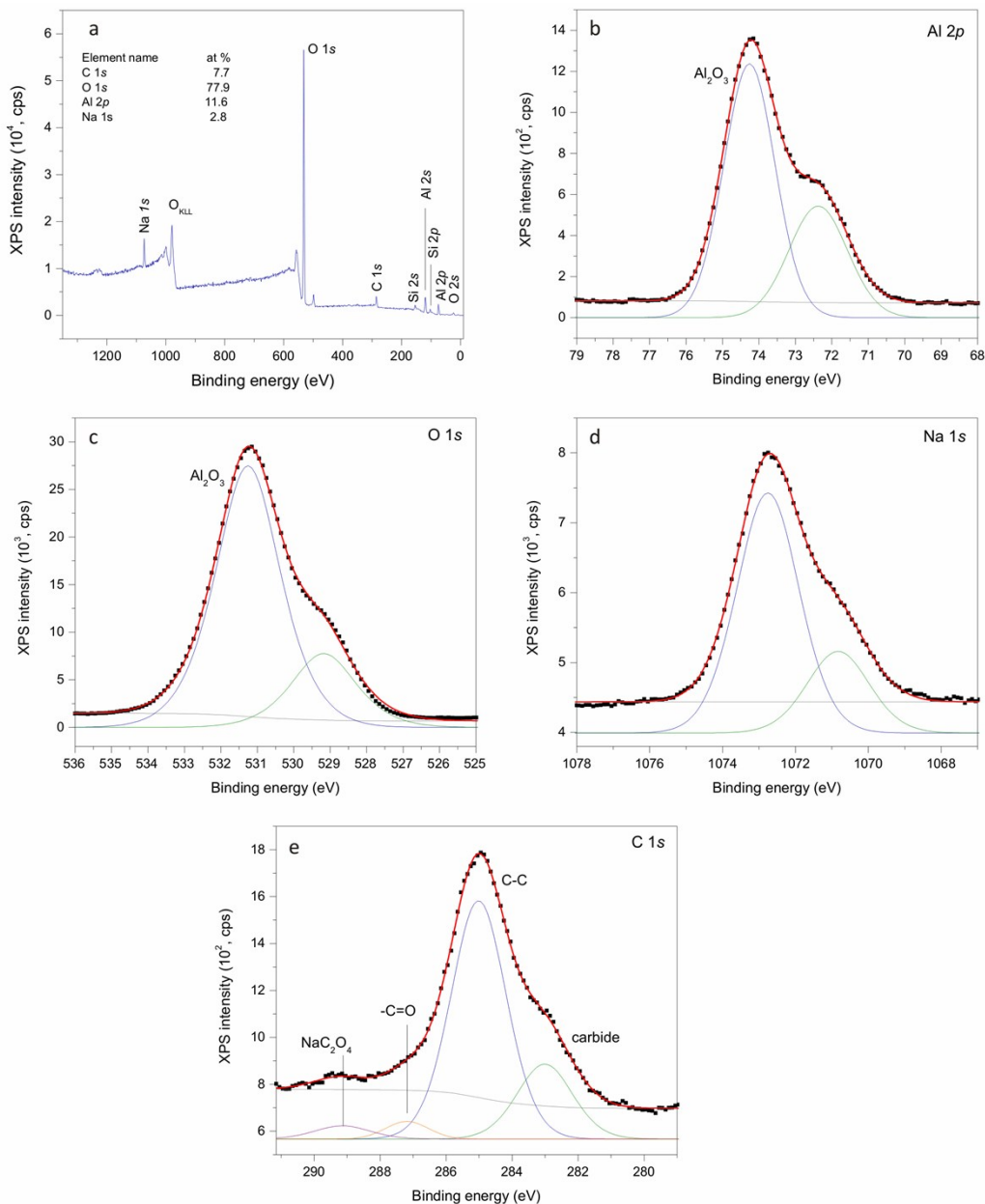


**Figure S3** XPS (a) survey spectrum, (b) Al 2*p*, (c) O 1*s*, (d) Na 1*s* and (e) C 1*s* data measured on surface of $Al_2O_3$ sample.

*Sample 4 – Si/SiO₂/h-BN*

The measurement was taken at three different spots on the sample to attain an average over the heterogeneity of the sample. Figure S4a shows the survey spectrum revealing that nothing except Si, O, C, N and B exists on the surface of the sample.

The core level spectra of N 1s and B 1s are displayed in Figure S4b and S4c, respectively. The only peak at B 1*s* spectrum at binding energy of 190.3 eV can be associated with boron atoms in B-N bonds. Among the three spots on the measured surface, B 1*s* and N 1*s* were only spotted in one area, indicating a relative low ratio of BN and its heterogeneous occupation over the surface. The Figure S4d shows Si 2p core level spectrum consisted of one peak at 103.8 eV. This peak is actually undistinguishable doublet due to spin orbit splitting and corresponds to $SiO_2$[10]. No peak is detected attributing to Si in metallic form. The Si 2*p* signals come from the $SiO_2$ layers embedded with the BN. The C1*s* core level spectrum shown in Figure S4e reveals one chemical state, probably originating from adventitious carbon. The O 1*s* peak displayed in Figure S4f at binding energy near 533.3 eV can be associated with the oxygen atoms in $SiO_2$ bonds.
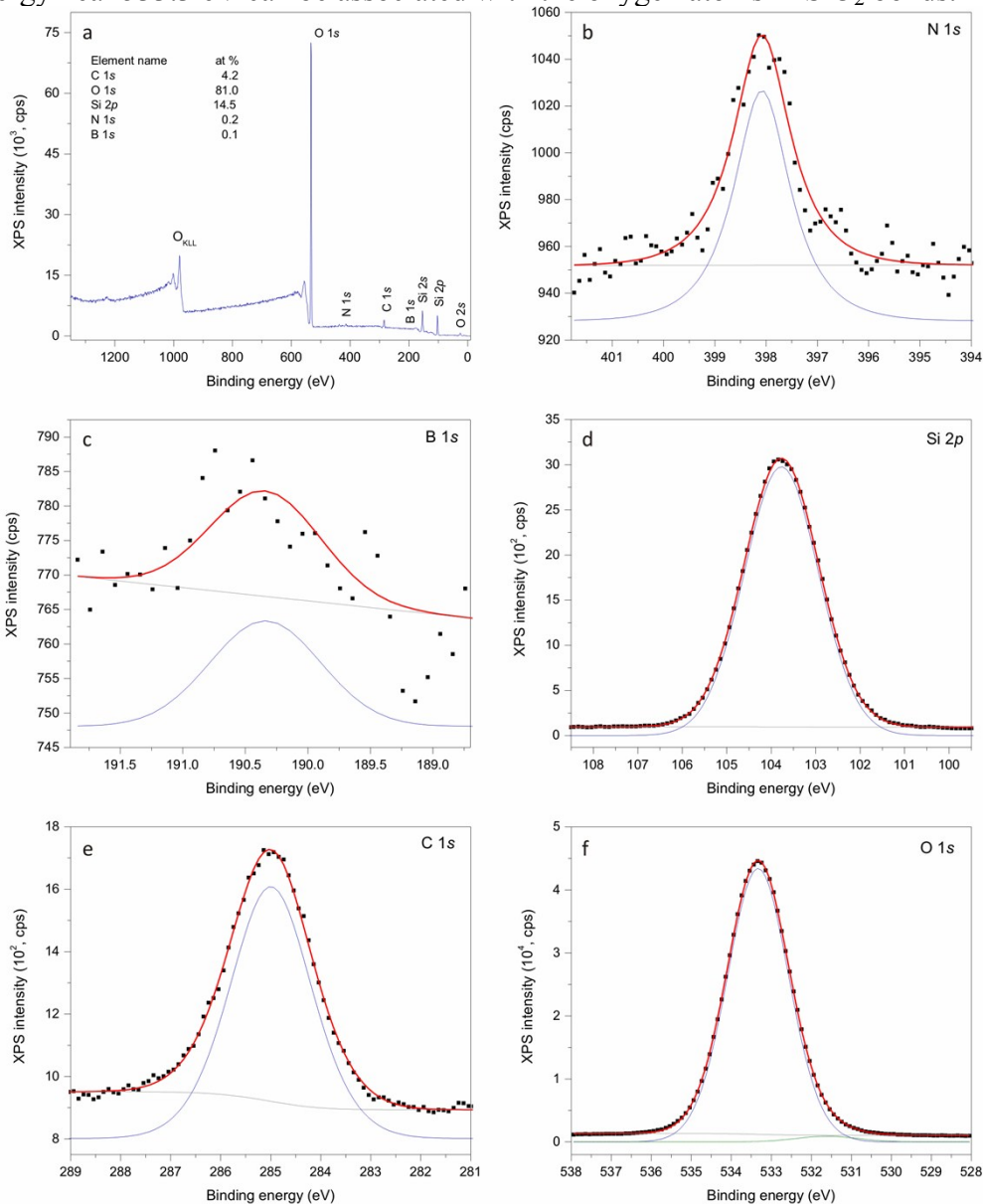


**Figure S4** XPS data collected on the surface of *Si/SiO₂/h-BN* sample: (a) survey spectrum and core level spectra of (b) N 1*s*, (c) B 1*s*, (d) Si 2*p*, (e) C 1*s* and (f) O 1*s* after deconvolution process. *Sample 5 O-MCD*
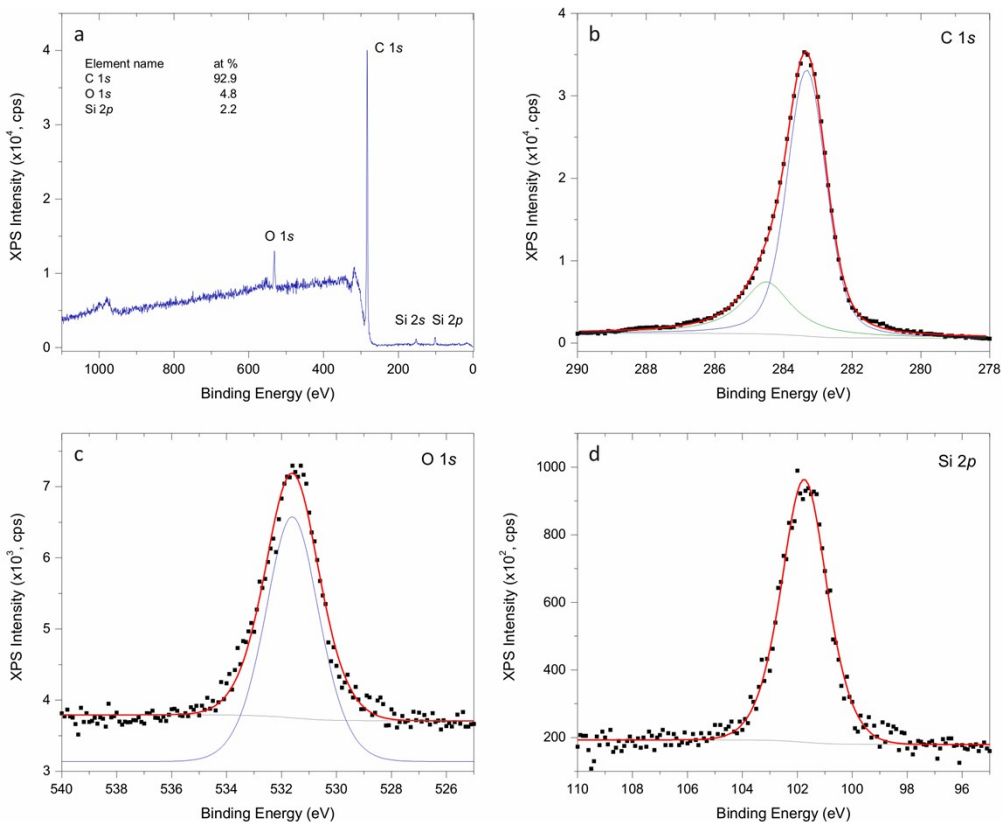
The XPS survey spectrum of O-MCD sample in Figure S5 reveals that the surface of the film contains only carbon and oxygen. This indicates that the surface of sample was clean from other contaminations (no N or F was detected). Core level C 1$s$ spectrum is deconvoluted using two peaks, centered around 284.5 and 287.2 eV, corresponding to C-C bond with sp$^2$ hybridization and carbon-oxygen bonds, respectively. One chemical state in oxygen O 1$s$ core level region with binding energy of 531.8 eV was observed due to the C-O bond.
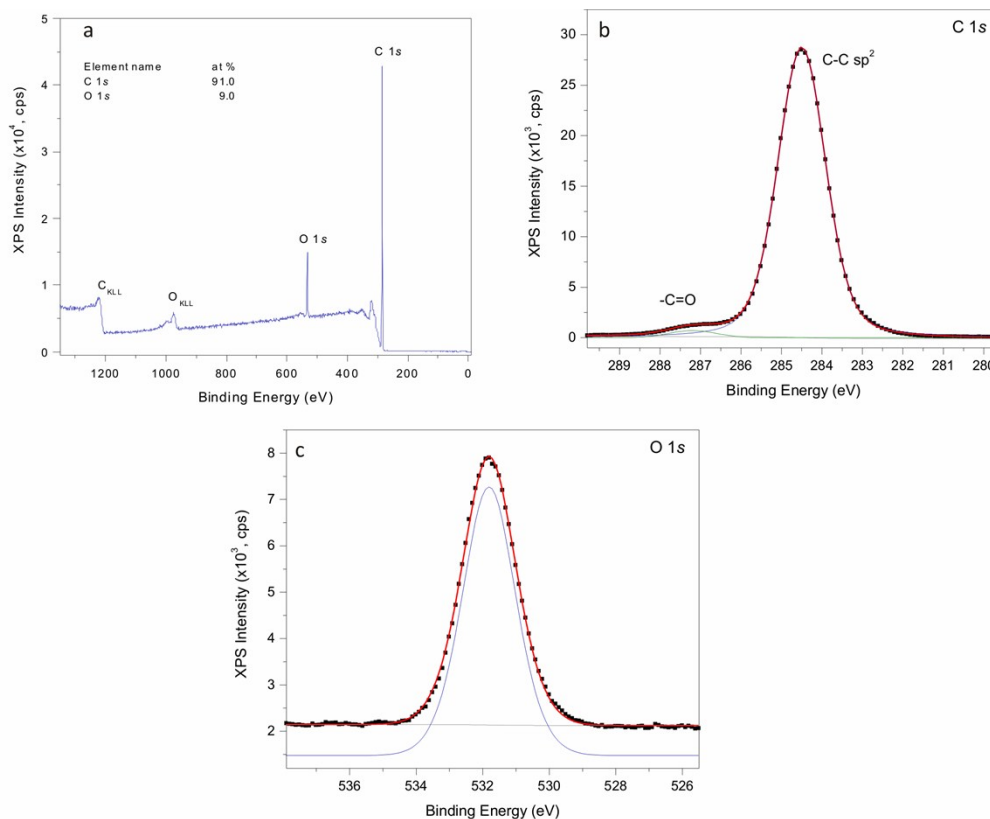


**Figure S5** XPS data collected on the surface of O-MCD sample: (a) survey spectrum, (b) C 1$s$ and (c) O 1$s$ deconvoluted core level spectra.

*Sample 6 – H-MCD*

The XPS survey spectrum measured on the H-MCD sample is shown in Figure S6. Note that this is the same sample presented above as "O-MCD", albeit after hydrogenation. Besides carbon and oxygen species we found a small amount of Si which is attributed to the high-temperature hydrogenation process itself (the plasma chamber interior can be observed through glass window-the Si source). The sample surface was therefore relatively clean from contaminations. In similarity to O-MCD, the core level C 1$s$ spectrum is deconvoluted using two peaks, and one chemical state was found for oxygen. Compared to O-MCD, this sample has nearly half the amount of oxygen on the surface (4.8 % vs 9.0 %).

**Figure S6** XPS data collected on the surface of H-MCD sample: (a) survey spectrum, (b) C 1*s*, (c) O 1*s* and (d) Si 2*p* deconvoluted core level spectra.

Based on the XPS data, and considering that all our samples were handled in ambient environment, we can conclude that they are essentially free of contamination.

## Current-Voltage characteristics

In order to confirm the result of oxidation and hydrogenation of the MCD we measured *I/V* on them. Figure S7 shows the typical result. Note that O-MCD showed no current for up to ± 30 V.
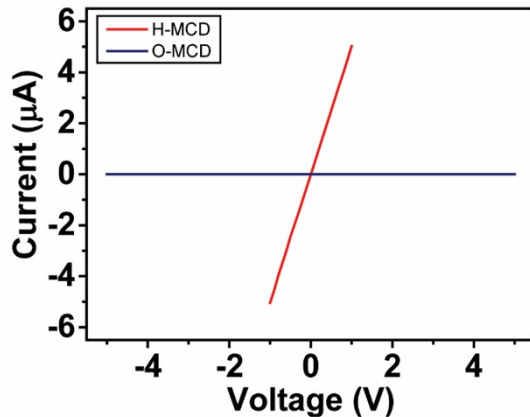


**Figure S7** *I/V* characteristics on H- and O-MCD.

**Atomic Force Microscopy**

Figure S8a,b shows detailed AFM topography of pristine sapphire before and after annealing in air at 1500 $^{o}$C, respectively. The larger terrace in Figure S8b is about 400 nm wide, which is about 8 times larger compared to the as-received state of the same sample (~50 nm). We show larger annealed image (1x1 μm$^2$ vs. 500x500 nm$^2$ of as-received) for better illustration of the variation in annealed terrace sizes.
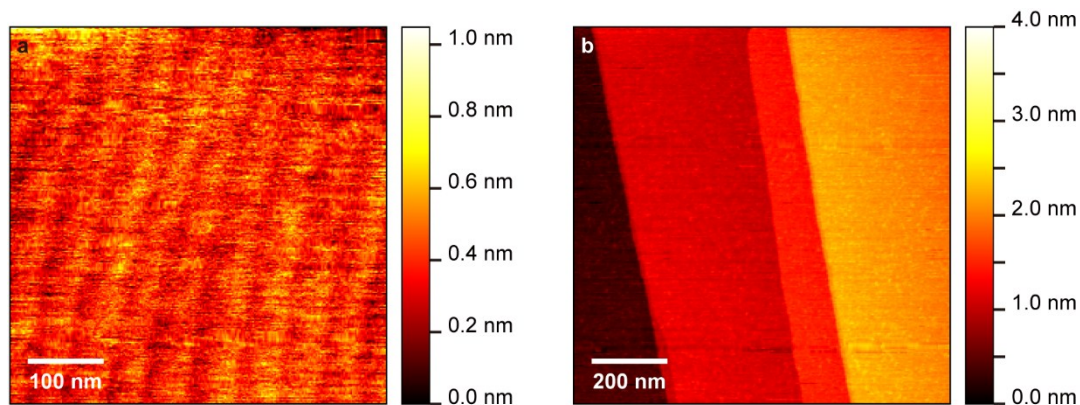


**Figure S8** (a, b) AFM topography of pristine sapphire before and after annealing in air at 1500 $^{o}$C, respectively.

Figure S9a,b,c shows AFM topography (500x500 nm$^2$) on pristine O-, H-MCD and h-BN surfaces, respectively. The polishing lines are clearly visible on O-MCD. Subsequent hydrogenation seems to have somehow affected the local morphology. Nevertheless, there was no impact in the RMS roughness of the surface which is about 0.05 nm in both cases.
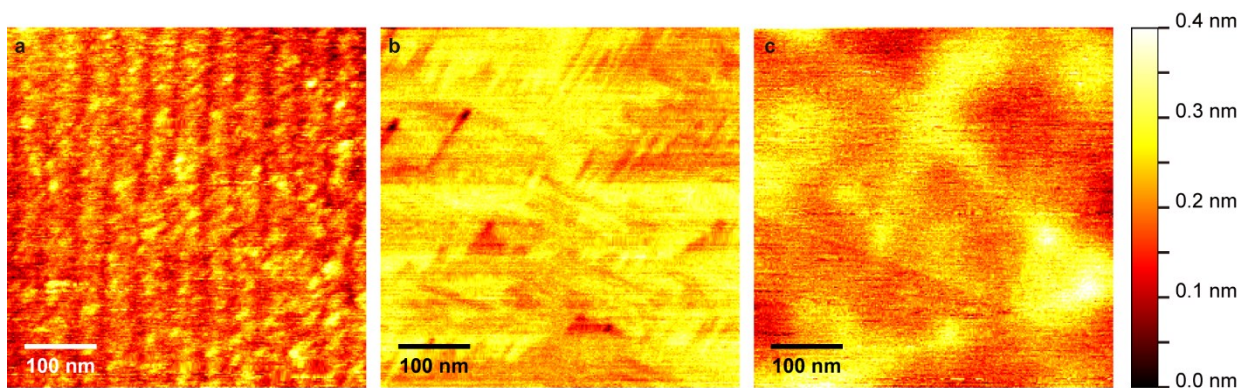


**Figure S9** (a, b, c) Detailed AFM topography on O-, H-MCD and h-BN, respectively.
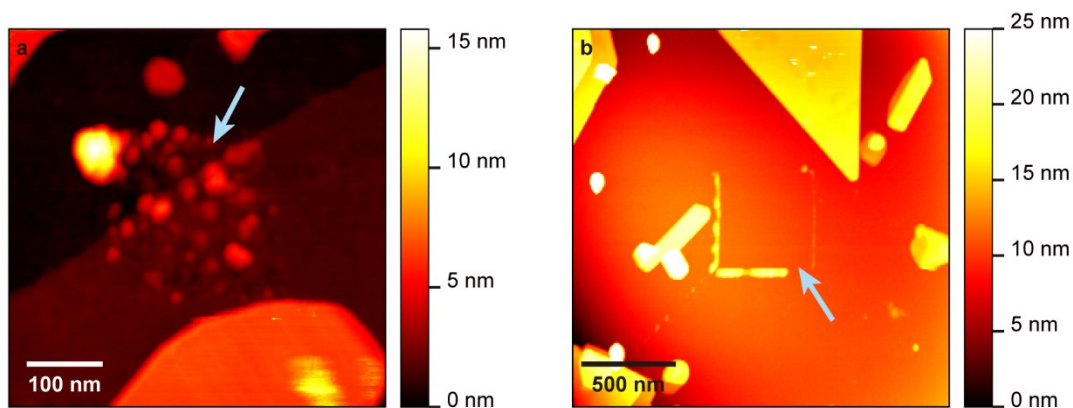
Figure S10 shows detailed AFM topography (500x500 nm$^2$) of a diacetylene island on sapphire. We can identify molecular orientation on the top part of the island.
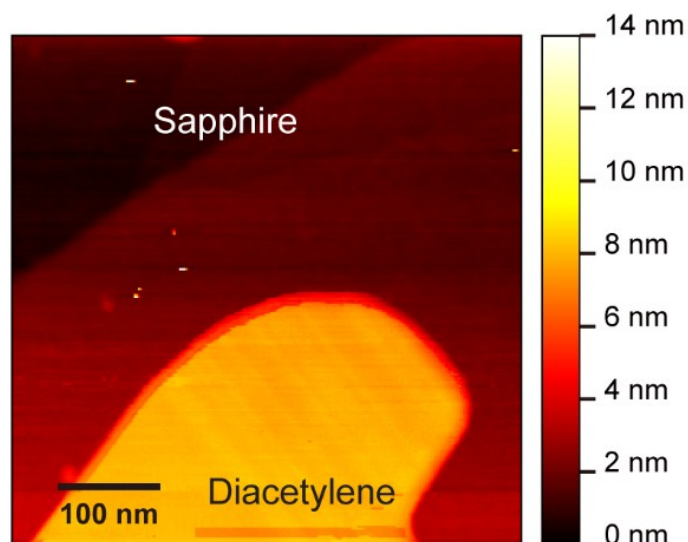


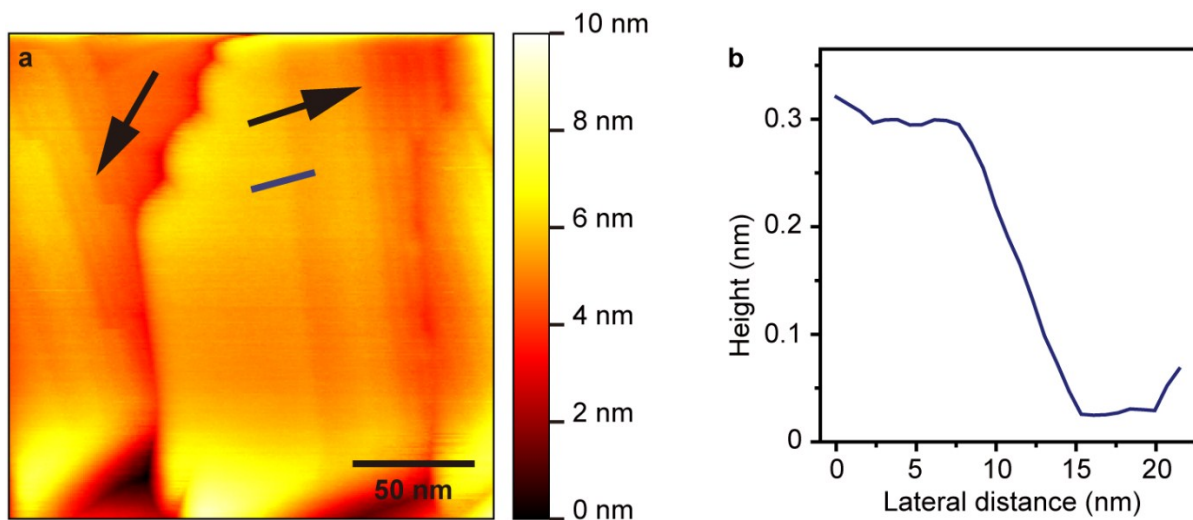**Figure S10** Detailed AFM topography of a diacetylene island on sapphire.

Figure S11a,b illustrates AFM topography on sapphire (500x500 nm$^2$) and O-MCD (2x2 μm$^2$), respectively, showing inter-aggregate areas after a CM scan in them. The CM scan sizes were 200x200 nm$^2$ on sapphire and 500x500 nm$^2$ on diamond. In the case of sapphire we see contamination particles spread all over the CM scan area. This indicates that there might have been few molecules assembled there before, which got disrupted by the scan. Solvent residue after dropcasting and ambient adsorbates are also adding to this effect, which is expected especially for hydrophilic surfaces treated in ambient conditions.

On O-MCD we see particles accumulated in the CM scan edges, while the area itself is clean. This shows that all molecules that were adsorbed/assembled in the area can be easily moved by the AFM tip. The molecules are therefore more weakly bound on the substrate in the case of O-MCD.



**Figure S11** (a, b) AFM topography on Sapphire and O-MCD, respectively, showing inter-aggregate areas after a CM scan in them. The arrows indicate the CM scan area.

Figure S12a depicts detailed AFM topography (200x200 nm$^2$) on a diacetylene aggregate assembled on H-MCD. We can see the layered structure of the aggregate in many places as denoted by the arrows. The spatial profile in Figure S12b, (measured on the area indicated by the blue line) shows that the height distance between those two adjacent layers is 0.3 nm. This equals the thickness of a single flat-lying diacetylene monolayer[11,12].



**Figure S12** (a) Detailed AFM topography on a diacetylene aggregate assembled on H-MCD. Arrows denote visibly multilayered areas (b) Spatial profile measured on the area indicated by the blue line in (a).

Figure S13a,b,c shows the phase shift images on sapphire, O- and H-MCD, respectively, after the deposition of diacetylene. In the case of sapphire and oxidized diamond two distinct adsorption states can be identified which indicate that aggregates and inter-aggregate space are composed of different materials, the latter being diacetylene-free. The H-MCD case is different, as the contrast is identical all over the image, suggesting diacetylene presence everywhere. This corroborates well with the proposed layered structure of the inter-aggregate areas on H-MCD. Different contrast on aggregate edges in Figure S13c is due to known AFM artifact when scanning fast over areas with abrupt height changes.
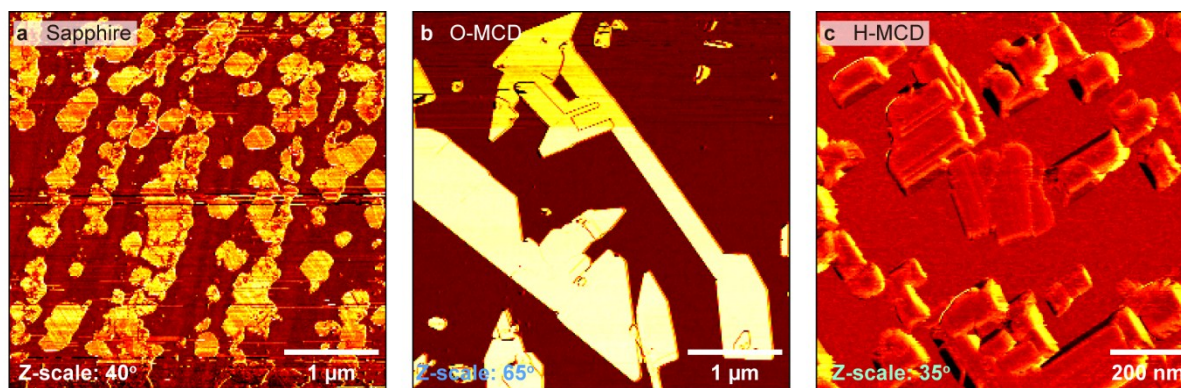


**Figure S13** (a, b, c) Phase shift images on sapphire, O- and H-MCD, respectively, after the deposition of diacetylene.

Figure S14a,b,c depicts optical images during contact angle measurements on sapphire, O-MCD and H-MCD, respectively. The measurements were performed by depositing a 1 μl deionized water droplet on the surfaces. The measured angles are 50.8°, 63.5° and 98.2°, respectively.

**Contact angle measurement**
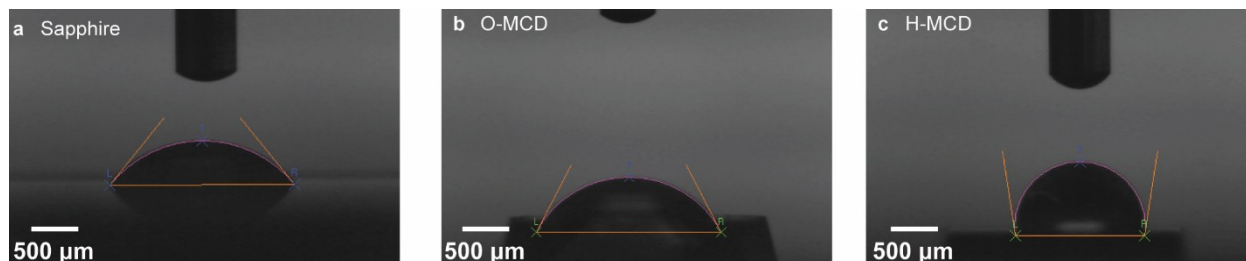


**Figure S14** (a, b, c) Optical images showing contact angle measurements on sapphire, O-MCD and H-MCD, respectively.

**Discussion**

One could critically point out that even though diacetylene assembles in a flat-lying manner on H-MCD, individual molecular chains are not resolvable in topography or phase shift images like on HOPG, $MoS_2$ and h-BN. The reason for this could be the large number of layers stacked on one another when forming an aggregate on H-MCD (40 nm of height protrusions correspond to ~130 layers) and also in the inter-aggregate area (where the layer count is unknown). We expect that this layering can effectively conceal the fine chain structure of diacetylene (typical topographical and phase variation within a monolayer are ~0.05 nm and < 1°, respectively) as the stacking is most likely not perfectly aligned. Another factor that can contribute to the lack of detailed structure is the different lattice structure of MCD (diamond vs. hexagonal on HOPG, $MoS_2$ and h-BN). It is noteworthy that deposition of diacetylene on H-MCD by a solution diluted up to 100 times, leads to the same type of high aggregates, albeit in smaller numbers. This means that the many-layer stacking is energetically favorable, and the reason for its occurrence is not the abundance of diacetylene molecules in the initial dropcasting solution.

Experimentation with diluted solution (up to 10 times) deposition on sapphire and O-MCD also showed aggregates similar to what is shown in the manuscript. On the other hand, increasing the concentration would surely lead to higher order aggregations due to the increased number of introduced molecules able to form stable, higher order islands. However as the stacking mechanism on those surfaces is already elucidated and does not result in flat-lying monolayer assemblies, further experimentation with higher solution concentration is irrelevant. For the same reason we did not allow the dropcasted droplet to dry on the surfaces but rather dried it shortly after impact.

Deposition of diacetylene in different temperatures was not performed due to the layer sensitivity to external excitations. Depositing at higher temperatures can give enough energy to the molecules to polymerize (Baking samples at 40 °C is enough). Lower temperature deposition on the other hand could potentially produce varied results but changes in the layer structure due to inherent changes in molecular mobility when moving samples from a low-T deposition area to

ambient (higher) temperature environment will also alter the layer. Therefore, characterization in air of samples prepared in lower-than-ambient temperature would lack consistency.

A 4 μl droplet of our solution contains $8.4\times10^{14}$ molecules (molecular weight of 10,12-nonacosadiynoic acid is 430.72). As the unit cell size of a flat lying SAM on HOPG is 7.5 nm × 0.47 nm and it contains 2 molecules[13], the molecular density of a monolayer is $5.7 \times 10^{11}$ molecules/mm$^2$. Assuming that the droplet expands over 2 mm$^2$, there are enough molecules to form about 700 monolayers all over that area. The reason we obtain thin layers on HOPG and MoS$_2$ is because 1) the solution expands over more than few tens mm$^2$ due to substrate hydrophobicity and long-range surface variations which cause the droplet to be quite mobile and leave the surface a few seconds after impact, and 2) the deposited molecular density is not homogeneous (i.e. coffee ring effect[14]). However, this is not the case in H-, O-MCD and sapphire, where the droplet stays over a small area, due to the negligible long-range surface variation of those polished substrates.

Further characterization of the diacetylene layers by spectroscopic and diffraction techniques is not possible to be realized two reasons: 1) our layers are deposited in air and thus on surfaces "wet" from ambient water adsorbed on them. Preparing those samples for any UHV-based measurement instantaneously destroys the molecular layer during the pressure changes. 2) Providing energy to the system (X-rays, laser beams, energetic electrons etc.) polymerizes the diacetylene, effectively altering the layer structure making it impossible to get further information on the structure of the assemblies as shown in the AFM images presented.

# References

[1] Briggs, D.; Seah, M. P. (Ed.), Practical Surface Analysis, Volume 1, John Wiley and Sons, Chichester, UK, 1990.

[2] http://www.kolibrik.net/science/kolxpd/

[3] Shirley, D.A. Phys. Rev. 1972, 5, 4709-4714.

[4] Cheung, T. T. P. X-ray photoemission of polynuclear aromatic carbon. J. Appl. Phys. 1984, 55, 1388-1393.

[5] Nozières, P.; de Domenicis, C. T. Singularities in the X-Ray Absorption and Emission of Metals. III. One-Body Theory Exact Solution. Phys. Rev. 1969, 178, 1097-1107.

[6] Buono, C.; Davies, P. R.; Davies, R. J.; Jones, T.; Kulhavý, J.; Lewis, R.; Morgan, D. J.; Robinson N.; Willock, D. J. Spectroscopic and atomic force studies of the functionalisation of carbon surfaces: New insights into the role of the surface topography and specific chemical states. Faraday Discuss. 2014, 173, 257–272.

[7] Kibsgaard, J.; Jaramillo, T. F.; Besenbacher. F. Building an appropriate active-site motif into a hydrogen-evolution catalyst with thiomolybdate [Mo$_3$S$_{13}$]$^{2-}$ clusters. Nat. Chem. 2014, 6, 248–253

[8] Li, B. L.; Luo, H. Q.; Lei, J. L.; Li, N. B. Hemin-functionalized MoS$_2$ nanosheets: enhanced peroxidase-like catalytic activity with a steady state in aqueous solution, RSC Adv. 2014, 4, 24256-24262

[9] http://www.xpsdata.com/al2o3.pdf

[10] Moulder, J. F. Handbook of X-ray Photoelectron Spectroscopy: A Reference Book of Standard Spectra for Identification and Interpretation of XPS Data, Perkin-Elmer, Eden Prairie, MN, 1992, ISBN-13: 978-0964812413

[11] Nirmalraj, P.; Thompson, D.; Molina-Ontoria, A; Sousa, M; Martín, N; Gotsmann, B; Riel, H. Nanoelectrical Analysis of Single Molecules and Atomic-Scale Materials at the Solid/Liquid Interface. Nat. Mater. 2014, 13, 947–953.

[12] Enevoldsen, A. D.; Hansen, F. Y.; Diama, A.; Criswell, L.; Taub, H. Comparative Study of Normal and Branched Alkane Monolayer Films Adsorbed on a Solid Surface. I. Structure. J. Chem. Phys. 2007, 126, 104703.

[13] Okawa, Y.; Akai-Kasaya, M.; Kuwahara, Y.; Mandal, S. K.; Aono, M. Controlled Chain Polymerisation and Chemical Soldering for Single-Molecule Electronics. Nanoscale 2012, 4, 3013-3028.

[14] Deegan, R. D.; Bakajin, O.; Dupont, T. F.; Huber, G.; Nagel, S. R.; Witten, T.A. Capillary flow as the cause of ring stains from dried liquid drops. *Nature* 1997, 389, 827-829.